Pile driving and submarine slope stability
a hybrid engineering approach

Lamens, P.; Askarinejad, A.

DOI
10.1007/s10346-020-01585-2

Publication date
2020

Document Version
Final published version

Published in
Landslides

Landslides (2021) 18:1351–1367
DOI 10.1007/s10346-020-01585-2
Received: 6 May 2020
Accepted: 17 November 2020
Published online: 4 December 2020

P. Lamens · A. Askarinejad

Pile driving and submarine slope stability: a hybrid engineering approach

Abstract During pile installation into a submerged, sandy slope, liquefaction mechanisms including flow and cyclic liquefaction warrant attention. Because of the interconnection of these mechanisms, evaluating slope stability during and as a result of vibration-inducing construction activity is not trivial. This paper presents a practical approach to such an evaluation. The primary focus of any slope stability analysis must lie with flow liquefaction as the form of failure with the most hazardous potential. Given the importance of excess pore water pressure in giving rise to (delayed) slope failures due to cyclic loading events, excess pore pressure (EPP) generation and dissipation is the mechanism of most interest in modelling cyclic liquefaction. Currently, no engineering method exists which is able to capture the interconnected processes. Therefore, a hybrid model, consisting of a numerical tool which computes EPP generation and dissipation in time, is combined with empirical relations to describe the decay of EPPs generated due to pile driving in space and time. The proposed numerical tool predicts the evolution of EPP in a one-dimensional soil column close to a vibratory-driven pile, taking into account sustained static shear stresses, interim drainage, and pre-shearing. Radial EPP dissipation is considered the dominant mode of drainage. This engineering tool fits within a holistic slope stability analysis procedure, which is demonstrated for a submerged slope in the IJmuiden harbour of the Netherlands, where mooring piles and sheet piles are installed through a relatively loose layer of sand.

Keywords Pile driving · Coastal slope stability · Liquefaction · Flow slides · Vibrations

Notations

EPP	Excess pore pressure
CSL	Critical state locus
CSRL	Constant stress ratio line
CSR	Cyclic shear stress ratio
CRR	Cyclic resistance ratio
SSR	Static shear stress ratio
IL	Instability line
ESP, TSP	Effective, total stress path
TRX, DSS	Triaxial, direct simple shear
β	Slope angle
h	Slope height
N	No. of loading cycles
N_{liq}	Loading cycles to liquefaction
I_d	Relative density
ψ	State parameter
δ	Friction angle soil-pile interface
p, p'	Total, effective isotropic stress
q	Deviatoric stress
u	Pore water pressure
r_u	Relative excess pore water pressure
σ_{ij}, σ'_{ij}	Total, effective stress component
K	Coefficient of lateral earth pressure
η	Stress ratio q/p'
τ	Shear stress
ε_{ij}	Strain component
γ	Shear strain
G	Shear modulus
ν	Poisson's ratio
α	Rotation of principle stress axes
e	Void ratio
c_v, c_r	Vertical, radial consolidation coefficient
s_u	Undrained shear strength
ϕ'	Effective friction angle
r	Radial distance

Introduction

In various civil, geotechnical, and offshore applications, piles or sheet piles are installed into fully saturated sands, for example during the foundation installation of offshore wind turbines. Another common case is installation of (mooring) piles into submerged slopes along harbour or port embankments. A frequent concern when examining fully saturated un-cemented granular soils affected by vibrations is the potential for liquefaction. Any significant motion or excess pore pressure development may affect the stability of a slope through a (temporary) degradation of the soil strength.

Pile installation tests indicate that driving energy and frequency, as well as the type of stress wave induced in the soil, dominate the ground motion response in terms of vibration amplitude and attenuation (Jonker 1987; Massarsch and Fellenius 2008; Whenham 2011; Deckner et al. 2017). The particular motion of the soil as a result of shear waves emanating from the pile shaft is responsible for the generation of excess pore water pressure in soils, as also measured in granular soils in a limited number of other studies (e.g. Hwang et al. 2001; Meijers 2007). This link lies in the tendency of the soil to contract and undergo significant shear strain. Therefore, pile driving may create a zone of significant plastic behaviour or densification (Svinkin 2008). Pore pressure records reported by Lamens et al. (2020) indicate, however, that in sand, with a relatively high permeability, interim radial drainage is an important phenomenon to consider when examining vibratory pile driving. Unlike in most earthquake analyses, the situation under consideration may not be virtually undrained. This has further implications for the stability of a slope, which may alter over time as pore water migrates.

Theory and observations from the field measurements allow for several connections to be drawn between physical processes occurring in the sandy soil during pile driving. Figure 1 illustrates these connections. The distinction between liquefaction failure mechanisms as suggested by Robertson and Wride (1998), based

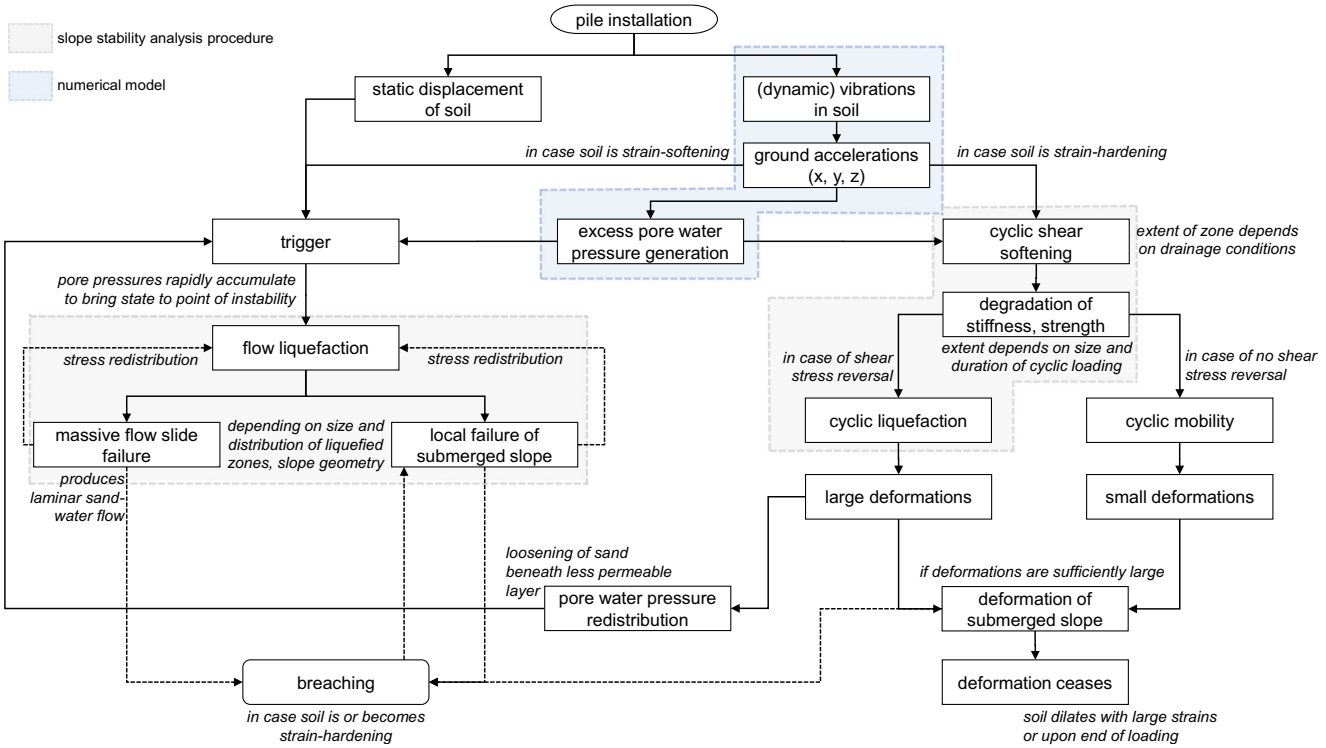

Fig. 1 Relations between pile installation effects, liquefaction phenomena, and slope failure mechanisms. The shaded areas highlight the two components of the engineering tool discussed in this paper: (1) a slope stability analysis procedure which allows for analysis of both flow and cyclic liquefaction and (2) a numerical model for excess pore pressure development

on the critical state soil mechanics framework, serves as a starting point.

Pile installation induces cyclic loading to a soil body. Cyclic loading may act both as a trigger for flow liquefaction, in the case of initially contractive soil, and as an antecedent to it, through the mechanism of cyclic liquefaction and subsequent pore water pressure redistribution, for initially dilative soil. This distinction is rooted in critical state soil mechanics as first introduced by Roscoe et al. (1958) and further elaborated in relation to soil liquefaction by, amongst others, Been and Jefferies (2015).

The consequences of pile installation for slope stability depend, amongst other aspects, on the zone affected by pile installation and the slope geometry. At times, it is possible to elucidate the type of failure post-event based on the time of initiation of the failure: a flow slide may occur *during* cyclic loading if the static shear stresses are high enough and the soil is loose enough. Flow liquefaction may also cause a failure after loading has ended due to the progressive nature of load redistribution (e.g. Boulanger and Truman 1996; Zhang and Askarinejad 2019a). Cyclic liquefaction, on the other hand, is a mechanism which always takes place during loading because it is driven by inertial forces.

In order to incorporate the three most important effects of vibrations emitted during pile driving on slope stability, namely (1) induced vertical and horizontal ground accelerations; (2) excess pore water pressure generation due to cyclic loading; and (3) a trigger mechanism for liquefaction, both static or flow liquefaction *and* cyclic liquefaction must be considered, with a primary focus on the first.

The state-of-practice liquefaction analysis procedure for slopes affected by dynamic loading typically involves three parts, carried out in the following order: (1) if liquefaction is triggered in significant zones of the earth structure, then analyse (2) the adequacy of post-liquefaction strengths in providing stability against a flow slide, in the absence of inertia forces, and (3) the level of seismic displacements relative to allowable deformations in a dynamic slope stability analysis using residual shear strength values where appropriate. Byrne et al. (2004) highlight that these processes are all part of a single response where pore pressure increase and liquefaction occur at different rates and times in various locations within the earth's structure. Redistribution of excess pore pressure may be detrimental for stability, but, eventually, dissipation and reconsolidation mean that the soil regains its strength. Not accounting for the interaction between these processes may be overly conservative, or non-conservative, depending on site conditions.

Although studies have been carried out which attempt to model the pore water response to pile installation or other vibrations related to construction in the near-field analytically (Randolph et al. 1979), or in terms of a threshold densification model (Dobry et al. 1981; Sawicki 1987; Matasović and Vucetic 1993); as well as redistribution of generated pore water pressure in time (Kokusho 1980; Malvick et al. 2006), currently no engineering method exists which is able to capture the interconnected processes outlined in Fig. 1, whilst allowing for an efficient evaluation to be made of the stability of a slope undergoing pile installation.

Under this consideration, this paper presents a holistic and practical slope stability analysis procedure comprised of a

combination of a soil strength framework and an approach for modelling liquefaction in slopes, taking into account empirically the redistribution of pore water pressure in space and time. The full-scale test at the IJmuiden sea lock, extending the access to the port of Amsterdam, the Netherlands, features as a case study.

Engineering tool

An advocated slope stability analysis procedure is presented in Fig. 2. The two types of liquefaction identified as part of Fig. 1, i.e. flow liquefaction and cyclic liquefaction, each require a different approach within slope stability analysis. Boulanger and Idriss (2011) highlight the importance of the order of slope stability analysis: the starting point of any assessment is the most significant failure mechanism in terms of suddenness and associated failure volume: flow liquefaction.

Step 1, flow liquefaction Flow, or static, liquefaction susceptibility is the primary analysis, carried out at the 'element' or constitutive level. Soil elements with relatively low confining pressures and high initial static shear stress at some depth below the face of the slope potentially lie close to a point of instability, and therefore form the 'unstable zone'. The instability line varies with initial state of the sand (e.g. Lade 1992). Figure 3 illustrates this for sands ranging from very loose (stress path no. 1) to loose (stress path no. 4). For dense sands, the stress path (no. 5) will move towards the constant stress ratio line (CSRL) as a result of loading.

When assessing the potential for liquefaction-induced failure in slopes, the *onset* of liquefaction is of interest (Askarinejad et al. 2015). Therefore, the strength parameters corresponding to this point of 'instability' serve as input. Static liquefaction represents a situation with undrained boundary conditions; an undrained shear strength ratio at yield represents the strength which statically liquefiable soils are able to mobilize before this onset (Zhang and Askarinejad 2019b; De Jager et al. 2017).

Chu et al. (2003), as Yang and Sze (2011) do in much the same way, relate the state of the soil to the critical stress ratio, or stress ratio at instability η_{IL}, which is the peak stress ratio during undrained triaxial testing for loose sands, and the peak stress ratio during drained triaxial testing for dense sands, see Fig. 4 for results for various sands. *State* is defined by the state parameter ψ, which

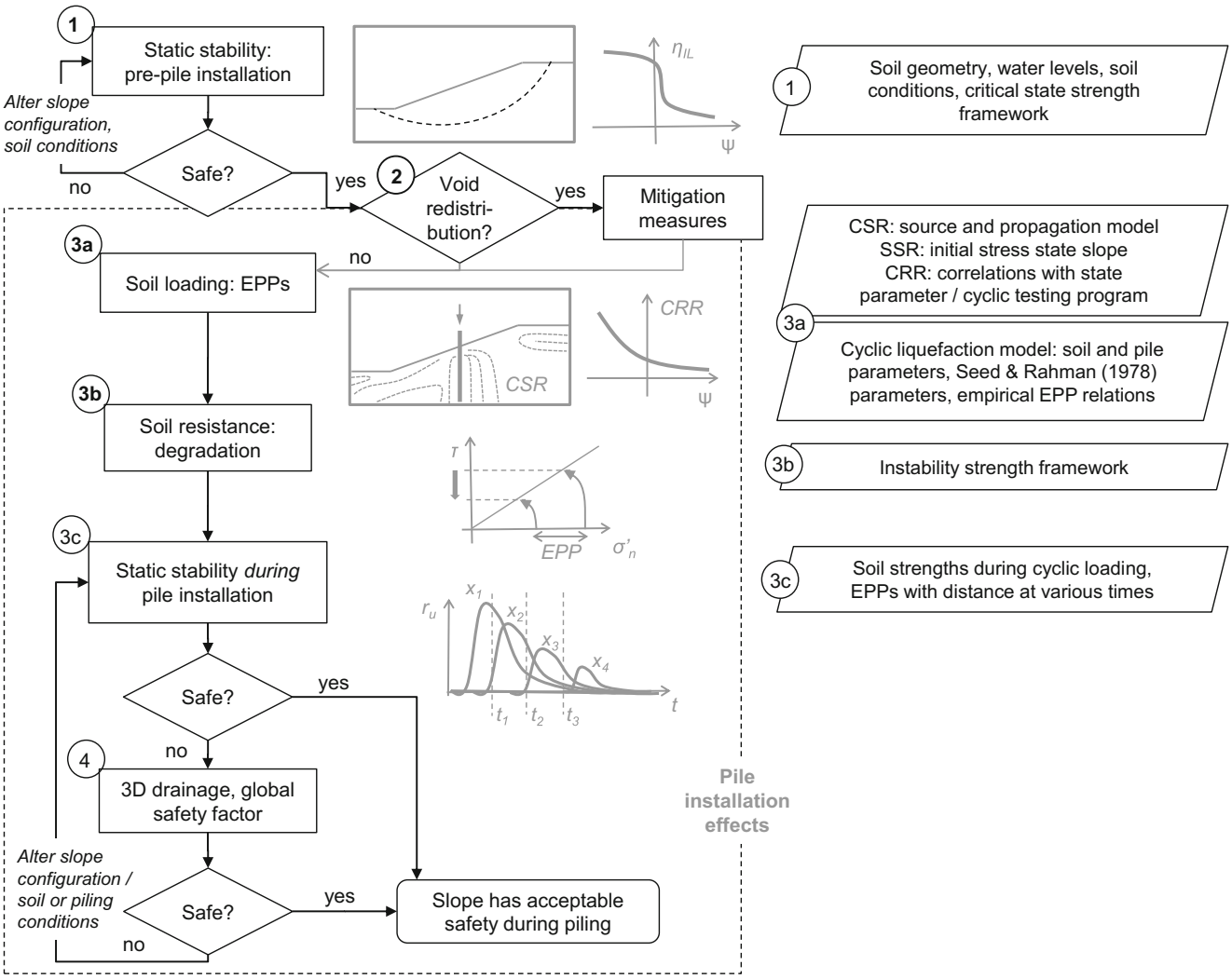

Fig. 2 Advocated procedure for evaluating the stability of a slope subject to pile installation. Inputs for each step of the procedure are shown on the right

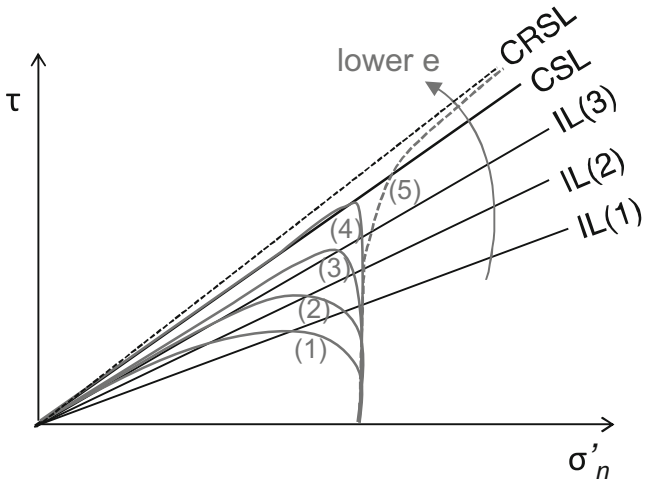

Fig. 3 Typical effective stress paths of very loose to loose sands (1–4) and dense sands (5) under undrained conditions

distinguishes between contractive and dilative soil behaviour, and captures both the initial density and the initial stress level: $\psi = e - e_c$, with e_c the critical void ratio. The modified state parameter ψ_{mod} is capable of reflecting potentially anisotropic consolidation condition by defining it *at* the peak mobilized strength, rather than at initial conditions. This reduces the potential for overestimation of liquefaction susceptibility (as $\psi_{mod} < \psi$).

The sustained static shear stress present in a slope is accounted for, too, in such a strength framework: the shear stress ratio, or SSR, may affect the direction of failure for strain-softening sands, whilst for strain-hardening sands it affects the mode of deformation and hence the extent of excess pore pressure development. Cyclic 'strength', often expressed in terms of a cyclic resistance ratio CRR, is not used as a strength parameter in the strength framework. Rather, it may be used to delineate between significant and insignificant EPP development close to the pile as a result of cyclic loading, since the process of EPP accumulation is

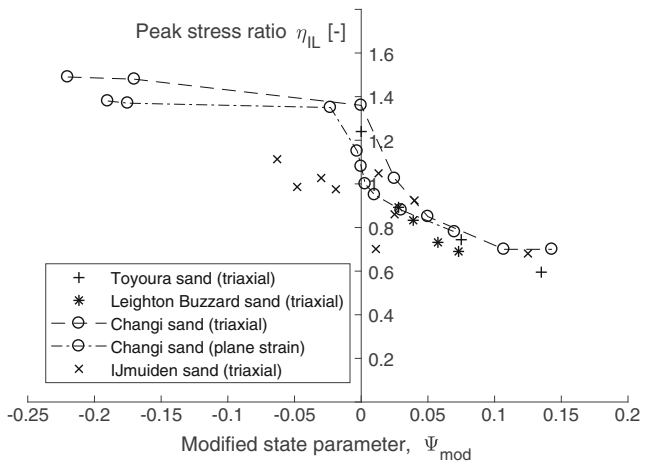

Fig. 4 Chu et al.'s (2003) instability strength framework for various sands: stress ratios at instability related to the modified state parameter, including values from literature and values derived from triaxial tests carried out on loose IJmuiden *Spisula* sand

considered the main driver of additional risk of slope instability due to pile installation.

A Mohr-Coulomb definition of yield or failure surface does not reflect non-linear soil behaviour leading up to the point of instability (e.g. Lehtonen and Länsivaara 2017). This is problematic both in limit equilibrium and finite element slope stability analyses. The use of the Cam-Clay like critical state-based constitutive model of NorSand, first developed by Jefferies (1993) and further developed since (Jefferies and Shuttle 2005), may be more appropriate in distilling peak stress ratios and peak undrained shear strengths at instability.

NorSand adopts an associated flow rule, nevertheless able to model realistic dilatancy through the introduction of capped hardening. It is a sparse model, able to describe the behaviour of sand based on the state parameter as all-encompassing state variable. NorSand parameters may be calibrated using triaxial tests. Calibration procedures are outlined in Bakhtiari (2006); Van den Eijnden and Hicks (2011); and Jefferies and Been (2015).

The calibrated NorSand model may be used to develop a strength framework for flow liquefaction, i.e. for monotonic shear loading in slopes. It is possible to define the strength at instability versus state in similar fashion to Fig. 4, in terms of a peak stress ratio. However, for direct input into limit equilibrium analyses using simple models such as Mohr-Coulomb, the definition of a mobilized undrained shear strength is more favourable in order to avoid the potentially dangerous overestimation of undrained shear strength when using effective stress parameters (Leroueil 2001). The undrained shear strength is dependent on the initial state and therefore, the relationship between the undrained shear strength mobilized at the point of instability and the initial state may be formulated in terms of undrained shear strength ratio s_u/p'_o versus the state parameter ψ.

In such a way, relatively simple shear strength models may be used within limit equilibrium or finite element stability analyses to determine the level of safety against flow liquefaction failure.

Step 2, void redistribution The excess pore pressure development during and after pile driving in sand partly depends on soil stratification, i.e. on the hydraulic confinement of the sand layer. Compared to the sand layer subject of Hwang et al.'s (2001) study, the sand layer in the Lamens et al. (2020) study showed that a less extreme confinement of the sand layer leads to a reduced potential for residual excess pore water pressure.

As indicated in Fig. 1, the redistribution of pore water pressure and, concurrently, that of voids may trigger liquefaction even after loading has ceased. The presence of silt or clay sublayers in the slope may inhibit the upward drainage of pore water and cause the development of an expansion zone at the base of an impermeable layer. The shear strength may deteriorate here locally—in extreme cases, a thin water film has been observed after seismic shaking (Kokusho 1999). Seed (1987) implicitly accounts for void redistribution in his empirical correlation between residual shear strength and pre-earthquake penetration resistance, based on the contributions of void redistribution to shear strength reduction in case histories.

The key consequence of void redistribution is that the undrained critical shear strength of a soil is not solely dependent on *initial* material properties and state, but can also reflect the response of a

system in its entirety (Kulasingam 2003). Therefore, an approach for evaluating slope stability, when void redistribution is expected to play a role given the local lithology, is to incorporate residual strengths, e.g. following Boulanger and Idriss (2011). This is a more conservative approach than using an instability strength framework.

In order to truly account for sand layer confinement or the effect of a relatively impermeable silty 'barrier' in slope stability analysis, a coupled stress-flow analysis is required. This allows simulation of water accumulation and the corresponding expansion zone. The fundamental mechanisms underlying void redistribution, however, are currently not well understood, agreed upon, or incorporated in engineering practice (e.g. Boulanger et al. 2014; Kokusho 2003; Seid-Karbasi and Byrne 2007; Malvick et al. 2008; Kamai and Boulanger 2010).

The slope stability analysis procedure proposed in Fig. 2 gives a practical engineering approach to consider void redistribution. Given that the safety against flow slides is sufficient, the potential for void redistribution in the slope may be qualitatively assessed in any dense-of-critical sand: (1) the sand layer must be susceptible to generation of significant EPP, i.e. it is cyclically liquefiable (CRR/CSR < 1.0); (2) the static shear stress is small relative to the cyclic shear stress amplitude (SSR/CSR < 1.0) (Malvick et al. 2006); and (3) the sand layer is known to be located between relatively impermeable layers, or there is an expected presence of silty/clayey layers and high levels of uncertainty about the spatial distribution of these layers. If the safety against flow slides is sufficient but close to critical, void redistribution is a mechanism which may render the stability critical.

Step 3a, EPP generation and dissipation during pile installation If void redistribution is deemed unlikely, only then are pile installation effects considered. The focus of these effects lies with cyclic liquefaction. Level ground at the crest and toe of the slope are more vulnerable to cyclic liquefaction due to a greater likelihood of shear stress reversal (Lee and Seed 1967; Vaid and Chern 1985; Byrne et al. 2004). The susceptibility of a slope to failure initiated by cyclic liquefaction requires a domain view rather than a soil element analysis: spatial variability and pore water pressure dissipation during and after cyclic loading play an important role through the phenomenon of void redistribution. This redistribution after loading ends can cause subsequent flow liquefaction (Robertson and Wride 1998).

NorSand is also suitable for simulation of the effect of cyclic shearing at soil element level, as Jefferies and Shuttle (2005) have incorporated softening of the yield surface following principal stress rotation. However, unless NorSand is incorporated into a fully coupled flow deformation analysis, the effect of cyclic liquefaction on slope stability is not modelled properly.

During cyclic liquefaction or mobility, the zone of maximum excess pore pressure generation may not be the loosest soil, but rather the soil that was in the most stressed location. Strength or stiffness may be reduced elsewhere as excess pore water migrates, leading to delayed failure. Jefferies and Been (2015) describe cyclic mobility as a boundary value problem requiring a fully coupled stress analysis, given that the phenomenon occurs within an entire domain and should not be assessed on the level of individual soil elements. Such an analysis is not trivial. Ideally, it would incorporate both flow and cyclic liquefaction, including the possible migration of pore water in time and space. Given that this concerns not only instability but also post-peak behaviour, i.e. the movement from a 'yield' to a 'critical' state, a sophisticated constitutive model must be integrated within the finite element method including considerations on localization of strains.

Strain localization and void redistribution are phenomena currently not sufficiently understood to be implementable in standard slope stability analyses. But given the evident importance of excess pore water pressure in giving rise to (delayed) slope failures due to cyclic loading events, EPP generation and dissipation is the mechanism of most interest in modelling cyclic liquefaction due to pile installation. The EPP development in space and time is the main input required for corresponding slope stability analyses. To this end, a hybrid model, consisting of a numerical tool which may compute EPP generation and dissipation in time in a one-dimensional soil column close to a pile, is combined with empirical relations to describe the decay of EPPs in space and time.

The main initial state variables which influence resistance to cyclic liquefaction are relative density, confining pressure, and static shear stress. The Seed and Rahman (1978) model for EPP generation directly accounts for the first two of these factors:

$$r_u = \frac{2}{\pi}\arcsin\left(\frac{N}{N_{liq}}\right)^{\frac{1}{2\theta}} \text{ where } N_{liq} = \left(\frac{CSR}{a \cdot I_d}\right)^{-\frac{1}{b}} \quad (1)$$

with r_u the relative excess pore pressure, or the excess pore pressure generated normalized for vertical effective stress; N the number of applied loading cycles; θ a constant for the rate of pore pressure increase, often taken as 0.7 for sands (Rahman and Jaber 1986); N_{liq} the number of cycles to liquefaction under undrained conditions; CSR the cyclic shear stress ratio; I_d the relative density of the soil; and a and b empirical parameters with values in literature around 0.3–0.5 and 0.2, respectively (Seed and Rahman 1978). The increment of generated pore pressure per time step $\frac{\partial u_{gen}}{\partial t}$ follows from:

$$\frac{\partial u_{gen}}{\partial t} = \frac{\sigma'_{vo}}{\theta \pi N_{liq}}\left[\sin\left(\frac{\pi}{2}r_u\right)^{2\theta-1}\cos\left(\frac{\pi}{2}r_u\right)\right]^{-1}\frac{\partial N}{\partial t} \quad (2)$$

This forms a suitable model to predict the pore pressure response to vibrations generated by (sheet) pile driving at a particular location in the slope when combined with a pre-shearing and a dissipation model. These two aspects allow for the effect of interim drainage to be accounted for. N_{liq} may be updated an empirical relationship following Smits et al. (1978) to account for changes in density and for changes in fabric upon pre-shearing. The dissipation may be implemented through a Terzaghi vertical consolidation formulation, taking into account radial dissipation with a correction factor A_{rad}, due to the one-dimensionality of the soil column considered:

$$\frac{\partial u}{\partial t} = \frac{\partial u_{gen}}{\partial t} + c_v\frac{\partial^2 u}{\partial z^2} + c_r\left(\frac{\partial^2 u}{\partial r^2} + \frac{1}{r}\frac{\partial u}{\partial r}\right) = \frac{\partial u_{gen}}{\partial t} + A_{rad}c_v\frac{\partial^2 u}{\partial z^2} \quad (3)$$

The CSR term in Eq. 1 results from a source and propagation model of the ground vibrations generated by vibratory pile

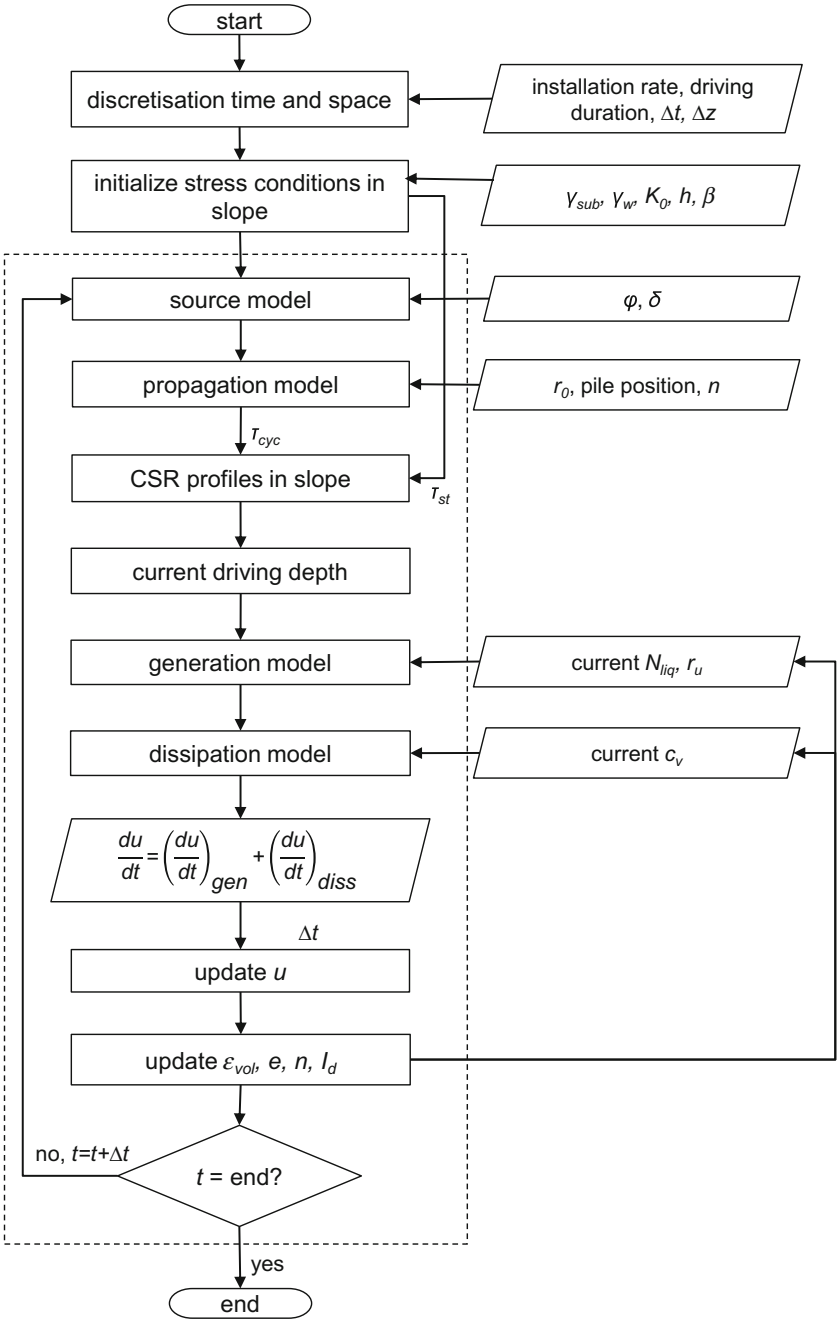

Fig. 5 Flow chart illustrating the structure of the program which implements the excess pore pressure development model

driving. It may be modelled as proposed by Meijers (2007). Cyclic shear stress (CSR) profiles are generated at the pile-soil interface where the soil yields. The attenuation of shear stresses is based on a shear stress or velocity amplitude model such as

$$\tau(r) = \tau_{\text{yield}}\left(\frac{r}{r_o}\right)^{-(n+\alpha_m)} \quad \text{where } \tau_{\text{yield}} = \sigma'_h \tan\delta \tag{4}$$

In which the shear stress τ is related to the radial distance from the source, r, using geometrical (n) and soil damping (α_m) attenuation coefficients. T_{yield} represents the shear stress at the pile-soil interface, where $r = r_o$, and is defined by the horizontal effective stress in the soil σ'_h and the angle of friction at the soil-pile interface, δ. These relations allow simulation of the soil column response at various distances from the pile in the slope. Initial static shear stresses in the slope may be accounted for by considering the rotation of the principal stress axes, commonly denoted by the angle α. The cyclic shear stress causes a periodic rotation of the orientation of the principal stress axis, and this rotation is what drives cyclic soil behaviour and EPP generation (Boeije et al. 1993).

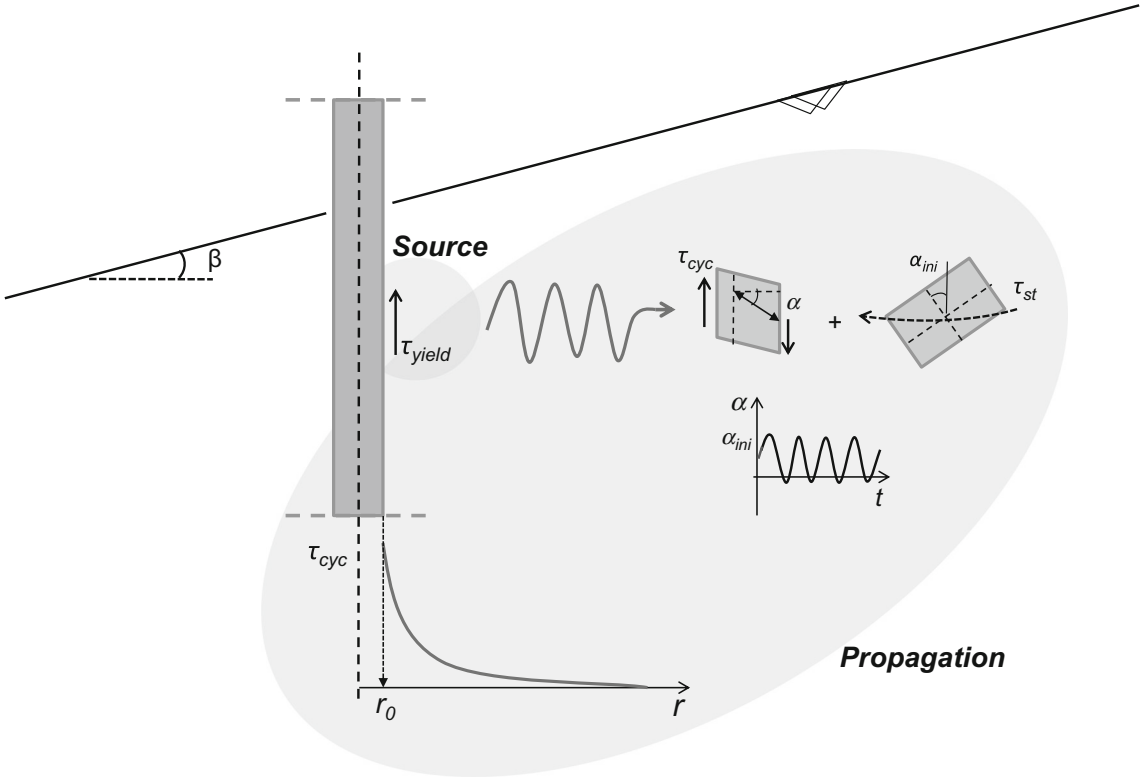

Fig. 6 Schematic visualization of source and propagation models

Figure 5 illustrates the implementation of the source and propagation model and the EPP generation and dissipation model within a simple one-dimensional numerical model. Figure 6 gives a schematic overview of the source and propagation model elements of the tool, whilst Fig. 7 gives a CSR distribution in slope of height 10 m, a slope angle 20°, a pile diameter of 1.6 m, an overall attenuation coefficient of 0.7, and a δ/ϕ'ratio of 0.67. The source and propagation model simulates the generation of vertically oriented shear waves originating at the pile-soil interface, and a separate modelling of the behaviour of the 'liquefied' zone close to the pile is not incorporated. Other assumptions underlying the source and propagation model include the disregard of stress waves emitted from the tip of the (sheet)pile, limiting the applicability to open-ended tubular friction piles and sheet piles installed in sand, and the disregard of the contribution of the volume of the sheet pile itself to changes in the surrounding soil volume.

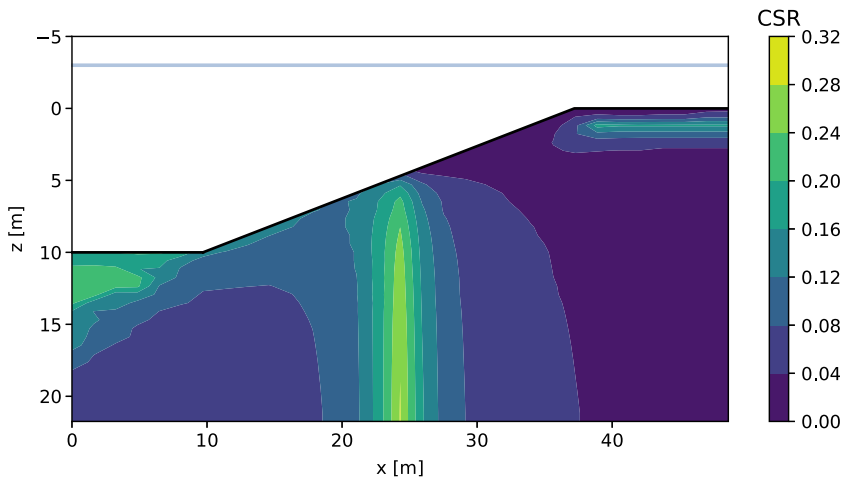

Fig. 7 Contours of CSR as generated by pile installation in the middle of a reference slope of height h 10 m, and with a slope angle β of 20°. The cyclic shear stress is based on high-frequency vibratory driving of an open-ended tubular pile, following a source and propagation model as proposed by Meijers (2007), and corrected for the presence of sustained static shear stress. The pile has penetrated fully over the vertical domain at this point

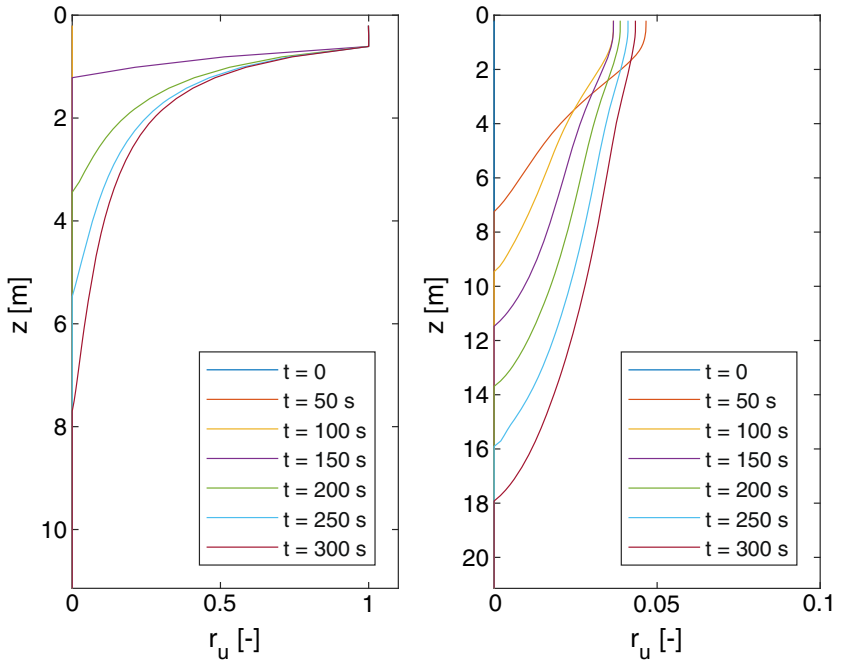

Fig. 8 Modelled excess pore water pressure development during pile installation in the middle of the reference slope in vertical profiles at the toe (left) and at the crest (right). z is the depth below the surface, r_u the relative excess pore water pressure. Installation rate = 0.03 m/s

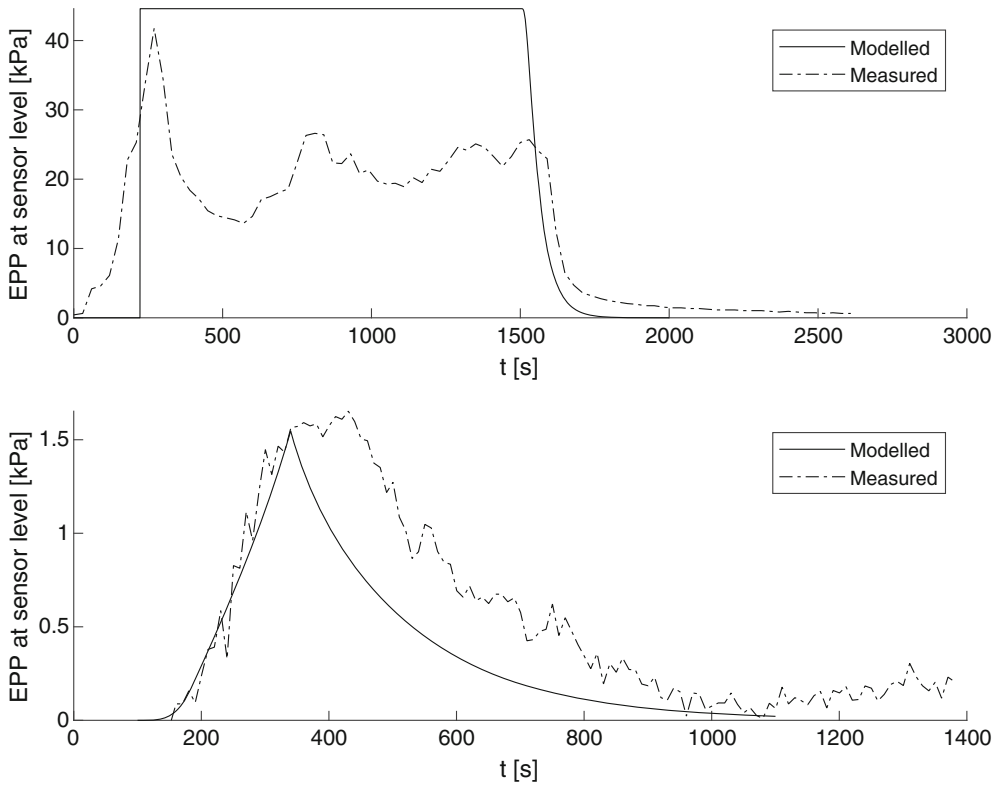

Fig. 9 Examples of validation of the one-dimensional EPP generation and dissipation model using measurements collected in IJmuiden, for the sensor located closest to the (sheet) pile

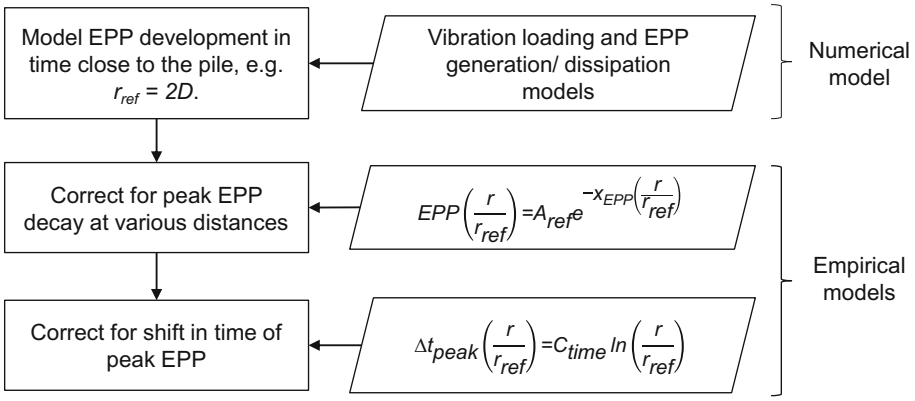

Fig. 10 Procedure for obtaining EPP development in time t at various distances r from the pile. A_{ref} is the amplitude of EPP modelled at a distance close to the pile; x_{EPP} is a factor which describes the decay of peak EPP in space; and C_{time} represents the time difference between the occurrence of peak EPP at various distances from the pile. After Lamens et al. (2020)

Figure 8 gives an example of EPP development profile for the crest of the slope in Fig. 7. Sensitivity analyses conducted using the model show that the toe of the slope is the most vulnerable region of the slope, and relative density is a key influencer of the pore pressure response. The slope angle and hydraulic conductivity have a less pronounced effect on pore pressure development. Other factors may also be studied, such as the effect of driving frequency and driving time, but Meijers (2007) reports that these factors are less critical than relative density in his settlement predictions.

The main limitation of the EPP generation model is that it is a one-dimensional model for stress state and excess pore pressure development, with consolidation in radial direction accounted for using a correction factor. This is a major simplification of three-dimensional drainage behaviour, which becomes clear upon validation of the program outlined in Fig. 5 with field measurements from IJmuiden. The modelling of EPP development close to the pile appears rather accurate, see Fig. 9. But the main implication of the model's one-dimensionality means that the radial flow of pore water is not truly accounted for; therefore, at distances further away from the pile, the peak EPP is generally underestimated and the time of occurrence of this peak EPP is not accurate.

Therefore, although the modelled EPPs might match those measured in the field at distances close to the pile shaft, a different approach may be required to model the EPP development in time at further distances from the shaft. Empirical relations for the decay of peak EPP with distance from the pile and for the time lag in occurrence of these peaks may be employed, e.g. following Hwang et al. (2001); or Lamens et al. (2020). The resulting procedure is summarized in Fig. 10.

Other reasons for deviation of modelled values from reality may include the speed of installation is modelled as being constant, whilst normally in practice the pile installation is almost continuously accelerating and decelerating; and any clay or silty layers are not accounted for in the model which assumes homogenous soil conditions, whilst these disturbance layers may affect the vertical and radial flow of pore water.

Step 3b, soil strength degradation Cyclic liquefaction and the pore pressure development in space and time are considered for those layers where CRR/CSR < 1.0. The effect of the pore pressure response on soil behaviour at any point in time during and after driving is a reduction of mobilizable shear strength. Figure 11 illustrates the stress path mechanism for this strength reduction. Therefore, modelled excess pore water pressures can either be input directly in a static slope stability analysis, e.g. in a finite element environment, or the pressures may be represented with the associated reductions in shear strength.

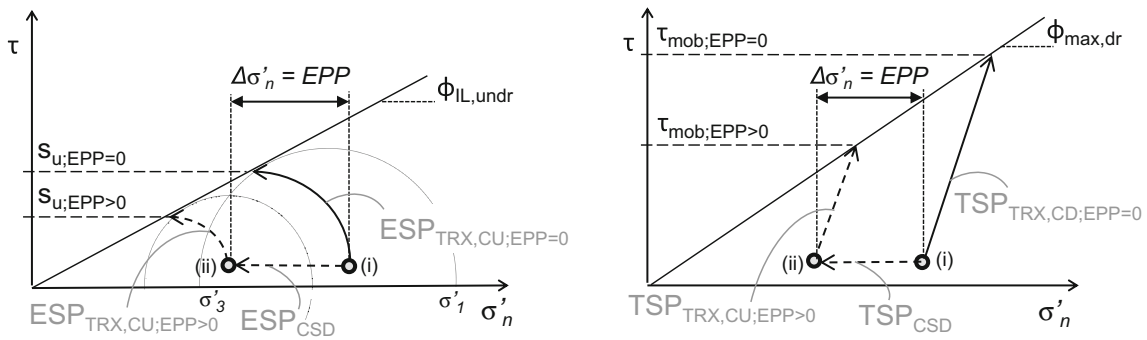

Fig. 11 Stress path mechanism for strength reduction as a result of excess pore water pressure, for contractive sands (left), and for dilative sands (right)

Step 3c, static slope stability analysis with EPPs In the case of vibratory pile driving in a sandy slope, Meijers (2007) has demonstrated that inertia-related or dynamic effects are of inferior significance with regard to slope stability compared to the diminishing of mobilizable shear strength due to excess pore water pressure development. Although cyclic liquefaction criteria may be used to determine the susceptibility of sand in slopes to cyclic liquefaction (e.g. Castro and Poulos 1977; Vaid and Chern 1985), in pile driving–related slope stability analyses, it is of essence to account for local development of pore water and its migration in time. Therefore, a static slope stability analysis may be conducted for various times during and after pile installation to capture a range of EPP situations within the soils.

Step 4, three-dimensional slope considerations Following the stability analysis of the slope incorporating EPP 'snapshots' in time, it may appear that the slope does not have a satisfactory factor of safety against failure for a certain duration in time. Due to the plane strain assumption underlying most 2D slope stability analyses, the excess pore pressures are modelled to exist infinitely far into the plane. In reality, EPPs dissipate not in two dimensions, but radially. This has a positive effect on global, or overall, slope stability. Therefore, using the known decay of peak EPP with radial distance from the pile, cross-sections may be taken at several distances from the central pile axis, and an analysis may be conducted for these cross-sections individually. A global safety factor may be distilled from the results of the analyses in order to establish an overall factor of safety for a certain zone of influence. The extent of the reduction of factor of safety due to pile installation will therefore ultimately depend on the size of the considered zone of influence, which depends on the size of failure volume and the failure mechanism of interest for the engineer.

Case study: full-scale field test at IJmuiden

The methodology explained above is verified using the data from test piles simulating the mooring piles installed into submerged slopes as part of the construction of a new sea lock in the North of the Netherlands. The full-scale pile installation field test was performed in 2016 to gauge the spatial and temporal trends of vibrations and excess pore water pressures during vibratory and impact pile driving. Lamens et al. (2020) present an overview of the set-up of the field test and an analysis of obtained field measurements.

Description of test site A set of three hollow tubular steel piles and five sheet piles were installed into the submerged slope. Five geophones, placed at different radial distances from the piles at a constant depth, measured the ground acceleration in three perpendicular directions, whilst 4 transducers, placed at the same depth, recorded pore water pressure during and after driving activities. All of the piles were installed using vibratory equipment (in all but one case at high frequency), bar the very first pile, which was brought to its final depth using a hydraulic impact hammer following the vibratory driving.

The soils making up the slope consist predominantly of siliceous sand. A relatively thick sand layer containing *Spisula* shell fragments is confined by two thin clay layers. A typical soil profile at the test location is given in Table 1. A typical CPT profile is given in Fig. 12. From the CPT results, a variation in density may be inferred within the Spisula layer: − 8.5 to − 12.5 m a.s.l. contains

Table 1 Typical soil stratigraphy at site

From (m a.s.l.)	To (m a.s.l.)	Soil description
5	0	Loose, sandy fill
0	− 8	Dense dune deposit
− 8	− 8.5	Clayey transition layer
− 8.5	− 16	Spisula sand
− 16	− 17.5	Van Velsen clay
− 17.5	− 19	Basisveen peat
− 19	− 35	Dense Boxtel sands

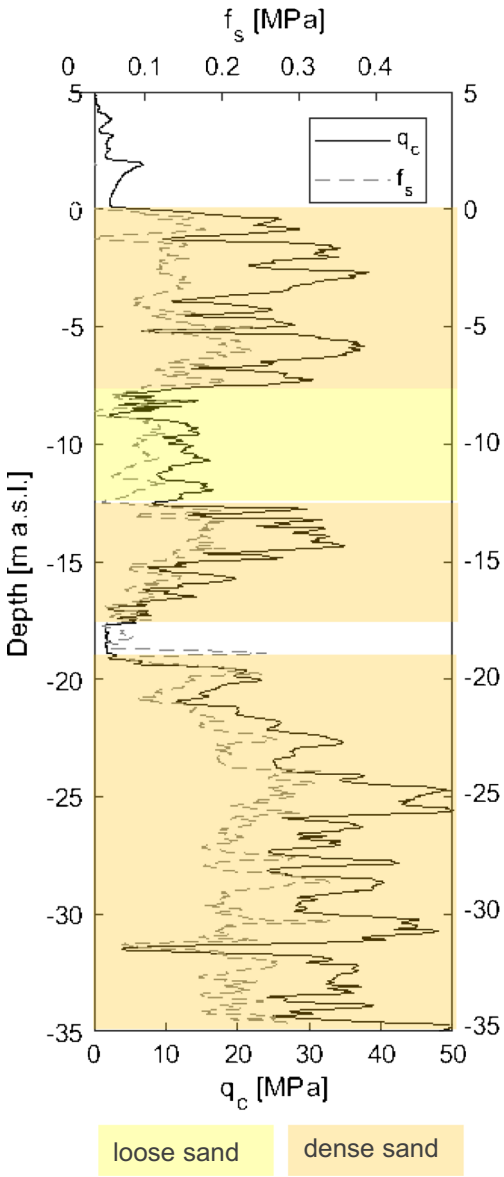

Fig. 12 A typical CPT performed at IJmuiden showing cone resistance q_c and sleeve friction f_s with depth

Table 2 NorSand parameter values for IJmuiden sands, and typical values for sands commonly encountered in literature

	Model parameter		Spisula sand
Critical state	Soil compressibility, slope CSL in e-ln(p') space	λ_e	0.06
	'Altitude' of CSL at $p = 1$ kPa	Γ	1.12
Plasticity	Critical friction ratio in triaxial compression	M_{tc}	1.25
	Volumetric coupling coefficient in stress dilatancy	N	0.2
	State-dilatancy coefficient in triaxial compression	χ_{tc}	4.5
	Plastic hardening modulus, often $f(\psi)$	H	$73–409\psi$
Elasticity	Dimensionless shear rigidity, G_0/p'	I_r	G_0/p', G_o from Eq. 6.8
	Poisson's ratio	ν	0.2

significantly looser sand than the bottom half of the layer. The monitoring instrumentation had an installation level of −10 m a.s.l., i.e. in the middle of this loose Spisula deposit.

Geotechnical properties of the Spisula sand layer Given its loose configuration as identified using the CPT data, the Spisula sand was investigated in particular detail. In geological terms, this layer is part of the offshore marine deposit belonging to the Blight Bank Formation. Borehole classification typifies the Spisula sand as a slightly silty, fine sand with thin layers of calcareous material. Analysis of the grain size distribution of 100 samples indicates that the uppermost part of the Spisula sand consists of fine sand; $D_{50} = 0.130$ mm on average. It is classified as a poorly graded sand with a uniformity coefficient ranging from 1.4 to 2.2. The silt fraction of the samples varies between 4 and 12%, whilst the carbonate content lies between 8 and 20%.

In situ dry and saturated unit weights for the Spisula sands are typically 14.5 and 18.5 kN/m^3, respectively. The minimum and maximum void ratios of the upper part of the Spisula sand, as determined through application of the ASTM method (D4253) to 50 samples, were found to be 0.6 and 0.9, respectively. With an average value of 2.60 for the specific gravity, the in situ relative density of the sand lies around 25%, which is classified as loose. The mechanical properties of the Spisula sand were investigated using consolidated drained and undrained triaxial tests according to ISO/TS 17892-9 (2004). Forty samples of Spisula sand were subjected to monotonic triaxial testing, of which Lamens et al. (2020) show some typical results in relation to liquefaction behaviour. The critical state friction angle was found to lie around 32°.

Step 1, flow liquefaction The drained and undrained triaxial tests performed on the Spisula sand result in a NorSand parameter set

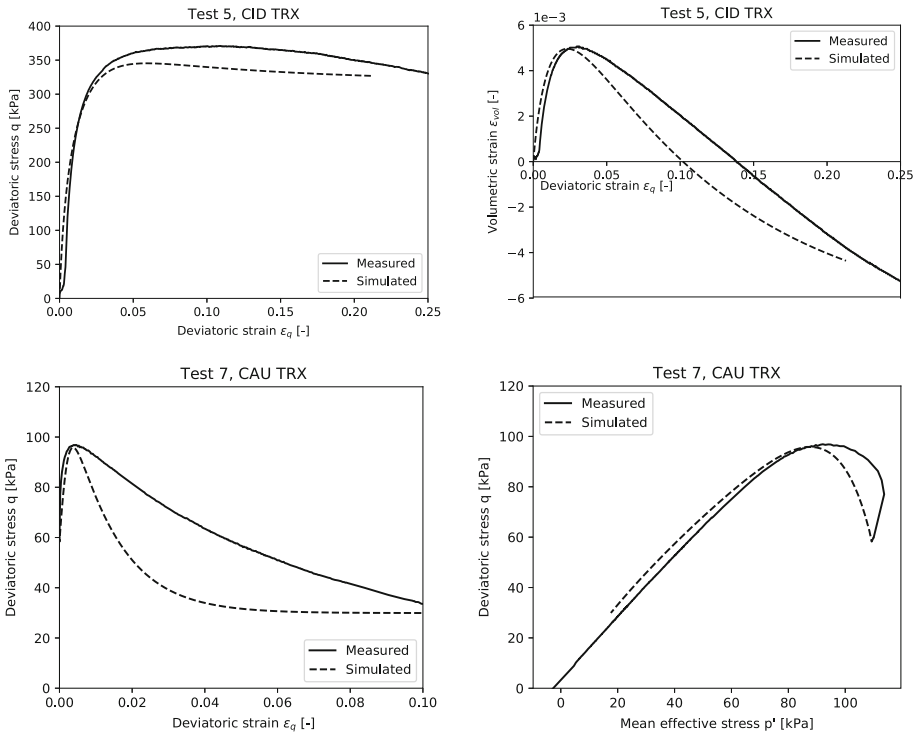

Fig. 13 NorSand simulations of drained (CID) and undrained (CAU) triaxial tests on IJmuiden sand using calibrated model parameters

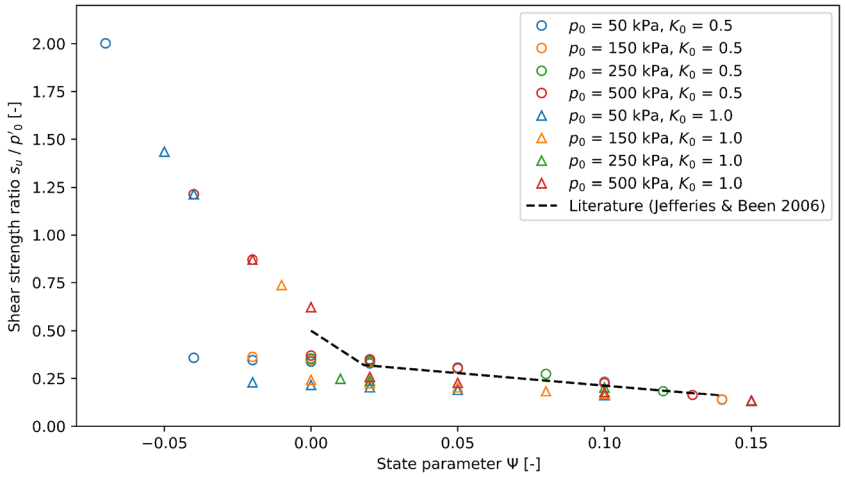

Fig. 14 Strength framework for flow liquefaction of IJmuiden sands in terms of undrained shear strength ratio for liquefiable sands, based on trends from NorSand simulations, triaxial tests, and literature. The 'literature' trendline is based on Fig. 6.21 of Jefferies and Been (2015), which incorporates an extensive set of triaxial test results on various sands

as in Table 2. The model parameters were calibrated based on several drained and undrained triaxial test results, two of which are shown in Fig. 13. The NorSand model is able to reasonably replicate undrained liquefaction behaviour observed in tests and delineates between a contractive and a dilative response. The stiffness response and volumetric behaviour are properly captured using the calibrated model parameters. The deviatoric strains as a result of the contractive response of the loose sample are captured up to the point of liquefaction.

From the NorSand simulations, it is evident that above a state parameter of − 0.07 the yield shear strength of the Spisula sand quickly diminishes. Therefore, sands with a state parameter $\psi > -0.07$ are classified as liquefiable and are consequently assigned 'undrained' peak shear strengths obtained from the undrained shear strength ratio, see Fig. 14. Peak friction angles, obtained from peak stress ratios, are only assigned to materials that may be considered non-liquefiable or drained, i.e. with a state parameter $\psi < -0.07$. To reduce the potential for overestimation of liquefaction susceptibility, the state parameters may be transformed to their modified version.

A static slope stability analysis is carried out for a typical slope at IJmuiden, of height 10 m and slope angle 20°. The soil stratigraphy is similar to that typically found in IJmuiden as in Table 1. Figure 15 gives the slope and soil profile with sand layers with varying relative density. Correspondingly, it shows the distribution of the initial state parameter. The associated strengths are based on the instability strength framework as presented in Fig. 14. Due to the lack of triaxial testing on the other types of sand present in IJmuiden, the strength framework derived from tests on Spisula sand is applied to all IJmuiden sands. Loose and dense sands adopt peak undrained and drained mobilized shear strengths, respectively, see Fig. 16a and b. The resulting safety against static slope failure is illustrated in Fig. 16c, which is output from a SLOPE/W (GeoStudio 2012) slope stability computation. The static stability analysis highlights that the majority of potential slip surfaces favour the statically liquefiable layer, giving an almost

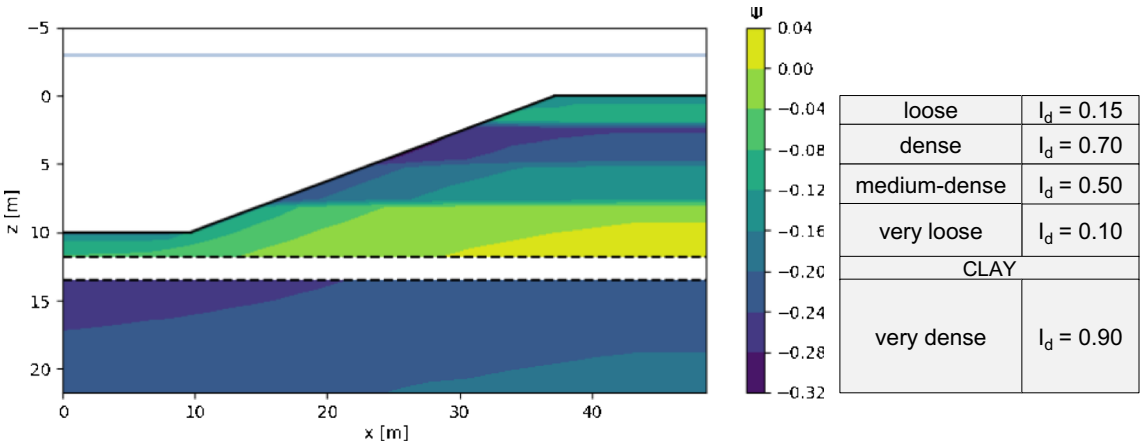

Fig. 15 Soil profile, and the corresponding distribution of initial state parameter, for use in slope stability analysis

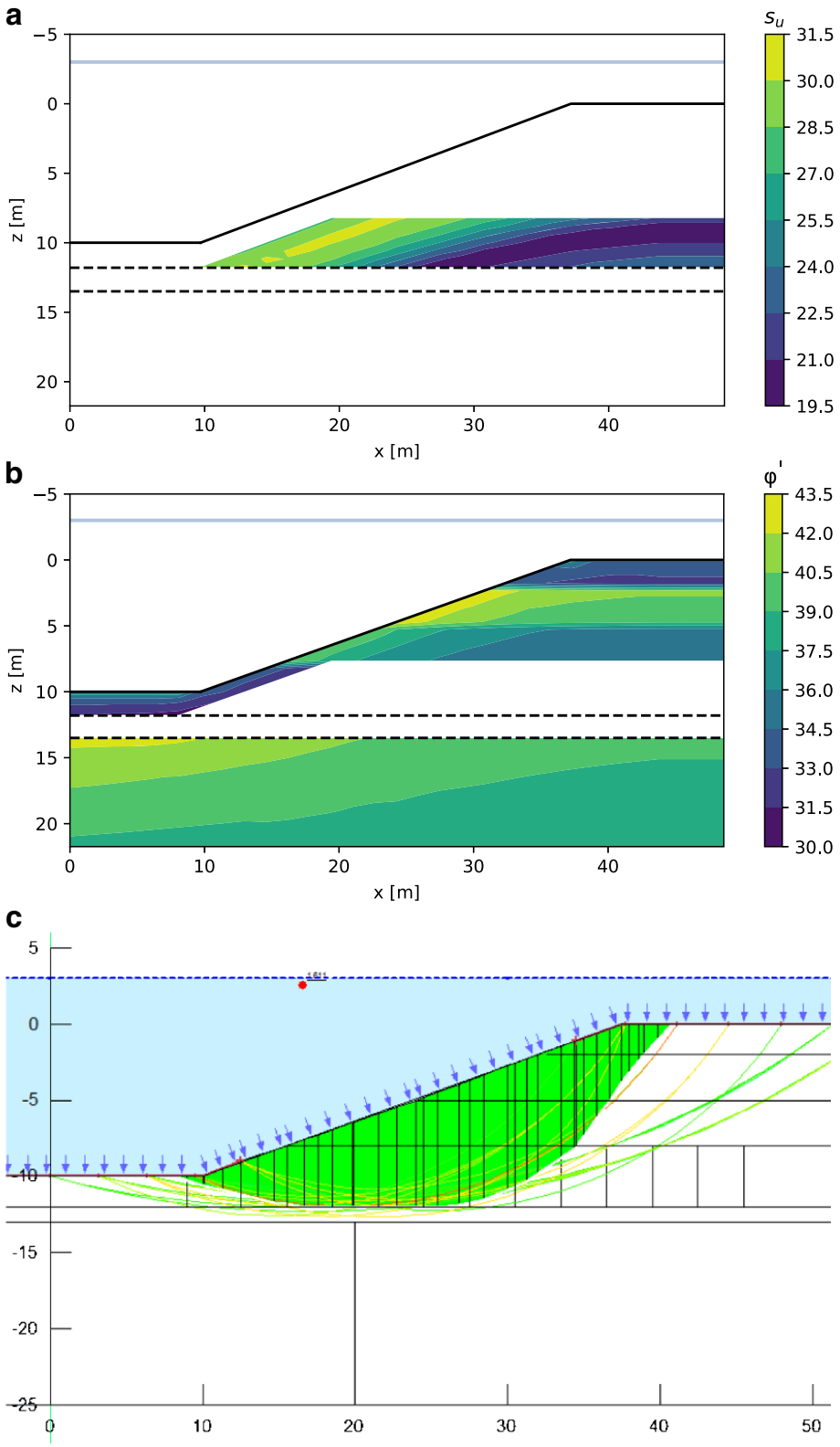

Fig. 16 Strength framework of Fig. 4 applied to static analysis of the reference slope prior to pile installation, accompanied by the corresponding SLOPE/W (GeoStudio 2012) slip surface analysis results. **a** Peak undrained shear strengths for liquefiable deposits. **b** Peak drained friction angles for non-liquefiable deposits. **c** Spencer slip surfaces for global slope failure mechanisms, with the critical slip surface outlined in white

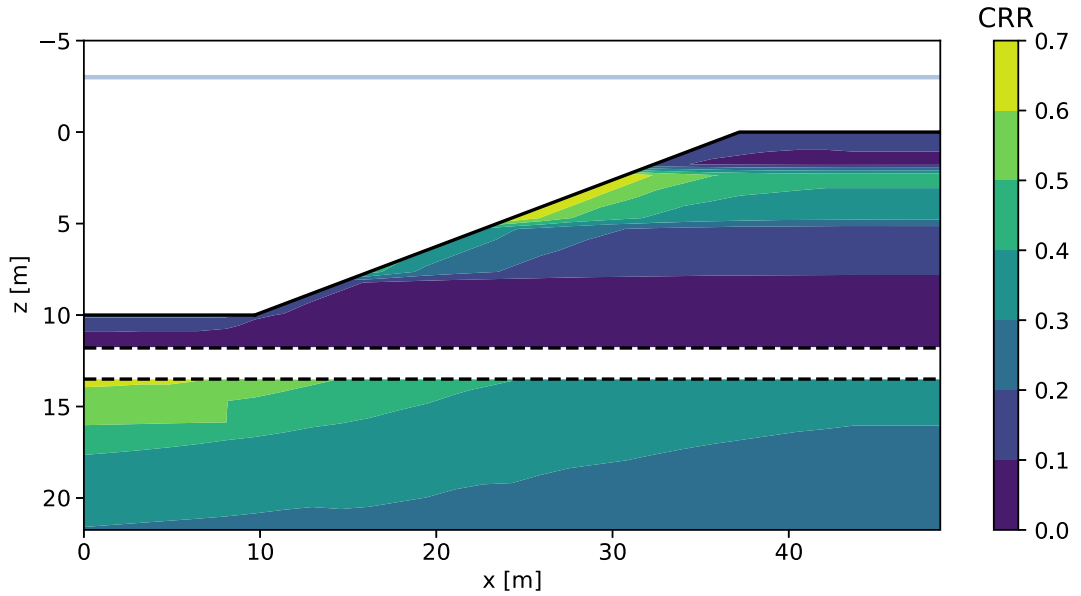

Fig. 17 Distribution of CRR values in the reference slope, related to the state parameter through $CRR = 0.03\ e^{-11\psi}$ (Jefferies and Been 2015)

horizontal critical slip surface through this layer—typical of a flow slide mechanism.

Step 2, void redistribution Given that the slope in the case study is not confined by clay layers both above and below the loose sand layer, void redistribution effects are not considered here. This is under the assumption that there is sufficient confidence in the location and extent of clay or silt layers and seams from site investigation.

Step 3a, EPP generation and dissipation during pile installation Figure 17 shows the distribution of CRR values in the slope, related to the state parameter through $CRR_{7.5} = 0.03\ e^{-11\psi}$ (Jefferies and Been 2015). Note that this relation holds explicitly for sands dense of critical.

This case study considers the installation of an open-ended tubular pile of diameter 1.6 m in the middle of this slope at a high frequency of 38 Hz, giving a combined attenuation factor $(n + \alpha_m)$ of 0.7, an installation time of 300 s, an installation speed of 0.03 m/s, and a pile-soil interface friction angle of $\frac{2}{3}\phi'^{\circ}$ in the sands. These pile installation specifications correspond to the CSR distribution shown in Fig. 7. Comparing the CSR and the CRR distributions it is found that, for this case, both the medium-dense and the loose layers are cyclically liquefiable.

The pore pressure developments in space and time in the middle of each of the cyclically liquefiable layers may be found through the hybrid numerical-empirical model as presented by Lamens et al. (2020). For the medium-dense layer, the resulting EPPs are presented in Fig. 18.

Step 3b, soil strength degradation The excess pore pressures are implemented in the slope stability computation by assigning the undrained shear strength reduction corresponding to the generated EPP in the middle of the of the medium-dense and loose sand layers. The reduced strengths are averaged over 1-m-wide sections.

Step 3c, static slope stability analysis with EPPs The stability of the slope is analysed in SLOPE/W (GeoStudio 2012), incorporating

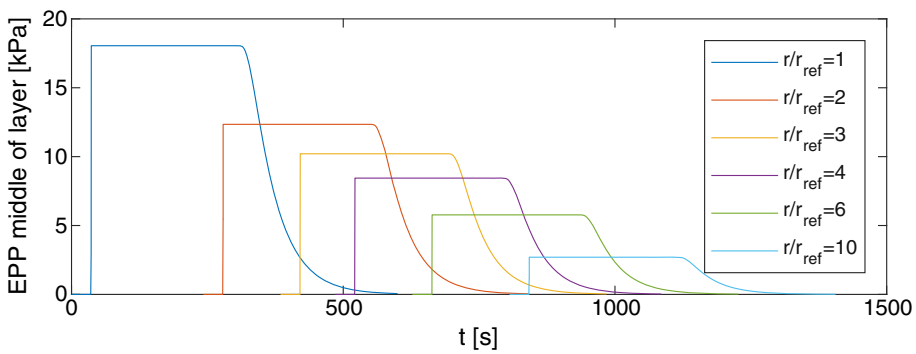

Fig. 18 EPP development in time in the middle of the medium-dense sand layer which is susceptible to cyclic liquefaction. r/r_{ref} refers to the radial distance from the pile, with $r_{ref} = 2D$

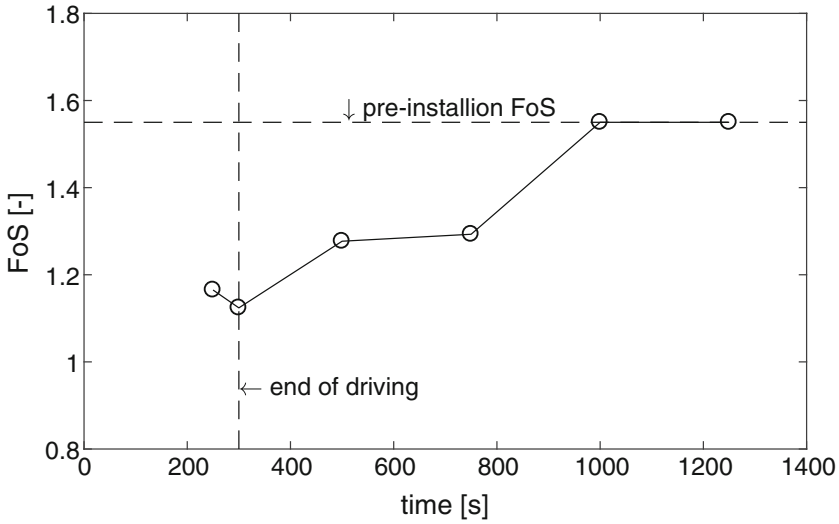

Fig. 19 FoS against deep-seated slope failure over time, as EPP distributions in the slope change

'snapshots' of the EPP at times of 250 s, 300 s, 500 s, 750 s, 1000s, and 1250s. The factor of safety against deep-seated slope failure at each of these 'snapshots' is presented in Fig. 19. The slope appears to be marginally stable between 250 s and the end of driving at 300 s (FoS < 1.2). The end of driving, at 300 s, is the most critical time. After 1000 s, sufficient pore water has dissipated to give minimal strength reduction along the critical slip surface, resulting in a FoS equal to that of the pre-pile installation stability analysis.

Step 4, three-dimensional slope considerations Figure 20 illustrates how the FoS against deep-seated failure increases with in-plane distance from the central pile axis. At a distance of six pile diameters and beyond, the FoS is equal to that of the slope in case of no pile installation effects. An assumption here is that radial decay of EPPs is considered the predominant three-dimensional effect on slope stability. The shearing resistance along the sides of the sliding mass, which traditionally distinguishes a two-dimensional from a three-dimensional slope stability analysis, is not examined here. This is a conservative approach.

Conclusions

In engineering practice, it is not possible to monitor for detection of flow liquefaction—given its sudden and devastating nature. Therefore, setting up an early warning system and observational methods are not applicable. In order to minimize the risk of a large-scale liquefaction failure during or after pile driving, a pre-emptive approach may be adopted. Based on the preceding investigation, and the use of the novel engineering tool described in this paper within a parametric analysis, a number of unfavourable

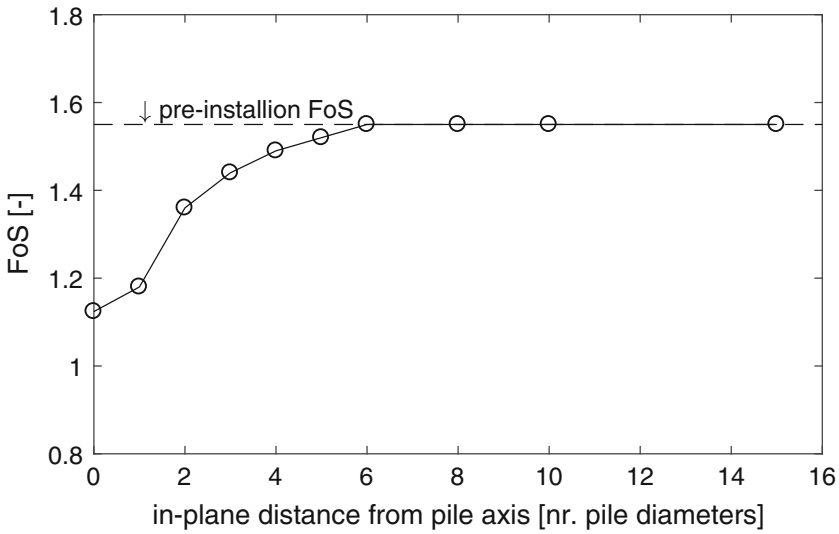

Fig. 20 Factor of safety (FoS) against deep-seated slope failure at various in-plane distances from the central pile axis, i.e. in the 3rd dimension, at pile driving time $t = 300$ s

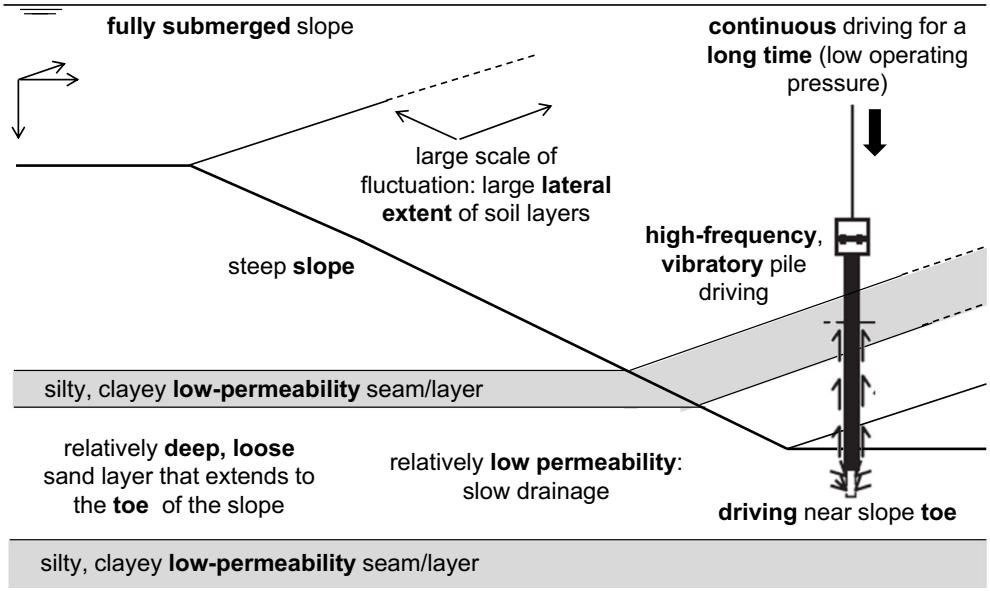

Fig. 21 Overview of unfavourable conditions which may render a slope susceptible to large-scale flow liquefaction failure during pile driving

conditions are identified and visualized in Fig. 21: submersion and a high slope angle renders the slope intrinsically more vulnerable to liquefaction failure; high-frequency vibratory driving has been shown to generate relatively large residual EPPs; continuous driving does not allow for enhanced interim drainage of pore water; the toe of the slope is relatively susceptible to cyclic liquefaction and the associated EPP development; and the presence of clayey or silty low-permeability soil layers or seams inhibits pore water drainage and may even contribute to delayed failure through a void redistribution mechanism. The number of conditions and extent thereof may provide an indication of the susceptibility of a slope to liquefaction failure and may support decision-making on mitigation measures.

When the decision is made to conduct further study on the susceptibility of a particular slope to liquefaction failure, the engineering tool subject of this study forms a novel pragmatic and efficient, and nevertheless scientific, first approach.

As part of the tool, a static pre-pile installation analysis, applying an instability strength framework rooted in critical state theory, precedes any consideration of pile installation effects: the phenomena of flow liquefaction, due to the presence of a sustained static shear stress in a slope, and cyclic liquefaction, due to pile installation, are treated separately. During cyclic loading events, EPP generation and dissipation is the mechanism of most interest in modelling cyclic liquefaction. It is important to note that residual post-pile installation shear strength is not uniquely related to pre-installation soil properties and state alone. Migration of pore water in time, and the possibility of void redistribution due to the presence of low-permeability layers or seams, raises the concern of 'delayed' failure.

A hybrid model, consisting of a numerical tool which computes EPP generation and dissipation in time in a one-dimensional soil column close to a vibratory-driven pile, taking into account sustained static shear stresses, interim drainage, and pre-shearing, is combined with empirical relations to describe the decay of EPPs in space and time. Radial dissipation is considered the dominant mode of drainage. Taking into account the diminishing of excess pore pressures in three dimensions within a slope stability analysis gives an indication of the spatial reduction in safety of the slope. For the case study used in this paper, the stability of the slope is only affected at a maximum of 6 pile diameters distance from the central pile axis.

The model and slope stability analysis procedure presented here do not account for void redistribution explicitly. An evaluation of whether this is conservative or non-conservative must be made as part of the procedure and be based on knowledge of site conditions. It also neglects the effects of the physical presence of the pile and the dynamic effects of the vibrations themselves, which form potential additions to this method.

References

Askarinejad A, Beck A, Springman SM (2015) Scaling law of static liquefaction mechanism in geocentrifuge and corresponding hydromechanical characterization of an unsaturated silty sand having a viscous pore fluid. Can Geotech J 52(6):708–720. https://doi.org/10.1139/cgj-2014-0237

Bakhtiari S (2006) Statistical characterization of spatial variability for a dredge excavation. MSc Thesis, University of Manchester
Boeije R, De Groot M, Meijers P (1993) Pore pressure generation and drainage underneath gravity structures. In The Third International Offshore and Polar Engineering Conference. International Society of Offshore and Polar Engineers
Boulanger RW, Kamai R, Ziotopoulou K (2014) Liquefaction induced strength loss and deformation: simulation and design. Bull Earthq Eng 12(3):1107–1128
Boulanger RW, Idriss IM (2011) Cyclic failure and liquefaction: current issues. In: Proc., 5th Int. Conf. on Earthquake Geotechnical Engineering. Chilean Geotechnical Society, Santiago, pp 137–159
Boulanger RW, Truman SP (1996) Void redistribution in sand under post-earthquake loading. Can Geotech J 33(5):829–834
Byrne PM, Park SS, Beaty M, Sharp M, Gonzalez L, Abdoun T (2004) Numerical modeling of liquefaction and comparison with centrifuge tests. Can Geotech J 41(2):193–211
Castro G, Poulos SJ (1977) Factors affecting liquefaction and cyclic mobility. J Geotech Geoenviron 103(6)
Chu J, Leroueil S, Leong WK (2003) Unstable behaviour of sand and its implication for slope instability. Can Geotech J 40(5):873–885
De Jager RR, Maghsoudloo A, Askarinejad A, Molenkamp F (2017) Preliminary results of instrumented laboratory flow slides. Procedia Eng 175:212–219
Deckner F, Viking K, Hintze S (2017) Wave patterns in the ground: case studies related to vibratory sheet pile driving. Geotech Geol Eng 35(6):2863–2878
Dobry R, Stokoe KH, Ladd RS, Youd TL (1981) Liquefaction susceptibility from S-wave velocity. In: ASCE National Convention. ASCE New York, New York, pp 1–8
GEO-SLOPE International Ltd (2012) Stability modeling with SLOPE/W 2012. GEO-SLOPE International Ltd., Calgary, Alberta, Canada
Hwang JH, Liang N, Chen CH (2001) Ground response during pile driving. J Geotech Geoenviron Eng 127(11):939–949
Jefferies MG (1993) Nor-sand: a simle critical state model for sand. Géotechnique 43(1):91–103
Jefferies MG, Been K (2015) Soil liquefaction, a critical state approach, 2nd edn. CRC Press, Abingdon, UK
Jefferies MG, Shuttle DA (2005) NorSand: features, calibration and use. In: Yamamuro JA, Kaliakin VN (eds) Soil constitutive models: evaluation, selection, and calibration, vol 128. Geotechnical Special Publication, ASCE, Reston, VA, USA, pp 204–236
Jonker G (1987) Vibratory pile driving hammers for pile installations and soil improvement projects. Proceedings of the offshore technology conference, Houston, TX, USA
Kamai R, Boulanger RW (2010) Characterizing localization processes during liquefaction using inverse analyses of instrumentation arrays. In: Hatzor YH, Sulem J, Vardoulakis I (eds) Meso-scale shear physics in earthquake and landslide mechanics. CRC Press, Leiden, pp 219–238
Kokusho T (1980) Cyclic triaxial test of dynamic soil properties for wide strain range. Soils Found 20(2):45–60
Kokusho T (1999) Water film in liquefied sand and its effect on lateral spread. J Geotech Geoenviron 125(10):817–826
Kokusho T (2003) Current state of research on flow failure considering void redistribution in liquefied deposits. Soil Dyn Earthq Eng 23(7):585–603
Kulasingam R (2003) Effects of void redistribution on liquefaction-induced deformations. PhD Thesis, Civil and Environmental Engineering Department, U.C., Davis
Lade PV (1992) Static instability and liquefaction of loose fine sandy slopes. J Geotech Eng 118(1):51–71
Lamens P, Askarinejad A, Sluijsmans RW, Feddema A (2020) Ground response during offshore pile driving in a sandy slope. Géotechnique 70(4):281–291
Lee KL, Seed HB (1967) Drained strength characteristics of sands. J Soil Mech Found Div 93(6):117–141
Lehtonen V, Länsivaara T (2017) Advances in determining Δu and s u for limit equilibrium analyses. In: Landslides in sensitive clays. Springer, Cham, pp 237–247
Leroueil S (2001) Natural slopes and cuts: movement and failure mechanisms. Géotechnique 51(3):197–243
Malvick EJ, Kutter BL, Boulanger RW, Kulasingam R (2006) Shear localization due to liquefaction-induced void redistribution in a layered infinite slope. J Geotech Geoenviron 132(10):1293–1303
Malvick EJ, Kutter BL, Boulanger RW (2008) Postshaking shear strain localization in a centrifuge model of a saturated sand slope. J Geotech Geoenviron 134(2):164–174
Massarsch KR, Fellenius BH (2008) Ground vibrations induced by impact pile driving. International Conference on Case Histories in Geotechnical Engineering, p 3
Matasović N, Vucetic M (1993) Cyclic characterization of liquefiable sands. J Geotech Eng 119(11):1805–1822
Meijers P (2007) Settlement during vibratory sheet piling. Doctoral thesis, TU Delft, Delft, the Netherlands
Rahman MS, Jaber WY (1986) A simplified drained analysis for wave-induced liquefaction in ocean floor sands. Soils Found 26(3):57–68
Randolph MF, Carter JP, Wroth CP (1979) Driven piles in clay—the effects of installation and subsequent consolidation. Geotechnique 29(4):361–393
Robertson PK, Wride CE (1998) Evaluating cyclic liquefaction potential using the cone penetration test. Can Geotech J 35(3):442–459
Roscoe KH, Schofield A, Wroth AP (1958) On the yielding of soils. Geotechnique 8(1):22–53
Sawicki A (1987) An engineering model for compaction of sand under cyclic loading. Eng Trans 35(4):677–693
Seed HB (1987) Design problems in soil liquefaction. J Geotech Eng 113(8):827–845
Seed HB, Rahman MS (1978) Wave-induced pore pressure in relation to ocean floor stability of cohesionless soils. Mar Georesour Geotechnol 3(2):123–150
Seid-Karbasi M, Byrne PM (2007) Seismic liquefaction, lateral spreading, and flow slides: a numerical investigation into void redistribution. Can Geotech J 44(7):873–890
Smits F, Andersen K, Gudehus G (1978) Stress-strain behaviour of Oosterschelde Sands: pore pressure generation. In Proceedings of the International Symposium on Soil Mechanics Research and Foundation Design for the Oosterschelde Storm Surge Barrier. Delft, The Netherlands
Svinkin MR (2008) Soil and structure vibrations from construction and industrial sources. Proceedings of international conference on case histories in geotechnical engineering, Arlington, VA, USA
Vaid YP, Chern JC (1985) Cyclic and monotonic undrained response of saturated sands. In: Proceedings of advances in the art of testing soils under cyclic conditions. ASCE Convention, Detroit, Michigan, pp 120–147
Van den Eijnden AP, Hicks MA (2011) Conditional simulation for characterizing the spatial variability of sand state. In Proc. 2nd Int. Symp. Comp. Geomech., Croatia (pp. 288–296)
Whenham V (2011) Power transfer and vibrator-pile-soil interactions within the framework of vibratory pile driving. Doctoral dissertation, University of Louvain, Louvain-la-Neuve, Belgium
Yang J, Sze HY (2011) Cyclic behaviour and resistance of saturated sand under non-symmetrical loading conditions. Géotechnique 61(1):59–73
Zhang W, Askarinejad A (2019a) Behaviour of buried pipes in unstable sandy slopes. Landslides 16(2):283–293. https://doi.org/10.1007/s10346-018-1066-1
Zhang W, Askarinejad A (2019b) Centrifuge modelling of submarine landslides due to static liquefaction. Landslides 16:1921–1938. https://doi.org/10.1007/s10346-019-01200-z

P. Lamens · A. Askarinejad (✉)
Faculty of Civil Engineering and Geosciences,
Delft University of Technology,
Delft, The Netherlands
Email: A.Askarinejad@tudelft.nl

P. Lamens
e-mail: pascale.lamens@gmail.com

P. Lamens
Royal Boskalis Westminster N.V.,
Papendrecht, The Netherlands